EDITORIAL CSIC

Materiales de Construcción
76 (361), January-March 2026, e401
ISSN-L: 0465-2746, eISSN: 1988-3226
https://doi.org/10.3989/mc.2026.412825

ARTICLE

Mechanical characterisation of 3D printed concrete masonry units with high aggregate and mineral addition content

Caracterización mecánica de unidades de mampostería de hormigón impresas en 3D con alto contenido de áridos y adiciones minerales

R.F. Nascimento
Federal University of Paraiba/UFPB, Civil Engineering Department (PPGECAM), (João Pessoa, Brazil)
Corresponding author: raquelfn96@hotmail.com, http://orcid.org/0000-0001-5376-9364

M.A.S. Anjos
Federal Institute of Education, Science and Technology of Paraíba, Civil engineering coordination/IFPB and Post-graduation in civil engineering/PEC-UFRN, (João Pessoa, Brazil)
marcos.alyssandro@gmail.com, https://orcid.org/0000-0001-9563-2534

J.P. Nascimento Júnior
Federal University of Paraiba/UFPB, Civil Engineering Department (PPGECAM), (João Pessoa, Brazil)
josivanjunior.j15@gmail.com, https://orcid.org/0009-0008-3010-8502

L.R. Pessoa
Federal University of Paraiba/UFPB, Civil Engineering Department (PPGECAM), (João Pessoa, Brazil)
leylapessoa01@gmail.com, https://orcid.org/0009-0002-4353-7062

L.S. Dias
Federal University of Paraiba/UFPB, Materials Engineering Department (PPCEM), (João Pessoa, Brazil)
leonardodiaspb@gmail.com, https://orcid.org/0000-0001-5925-2171

Abstract: The present study aims to expand the understanding of cementitious mixtures with low cement content and high levels of mineral additions and aggregates in order to assess their influence on the constructive characteristics of printing elements representative of structural masonry. The printing parameters and geometry of the pieces were defined to create a structure that can stand without internal bracing, with the goal of making the masonry construction process faster and simpler to print. In the hardened state, water absorption, the compressive and flexural strength of small pieces, as well as the compressive strength of 3DCP blocks and layer bonding, were evaluated. The results demonstrate that, for the parameters adopted in the printing system used, it is possible to construct volumetric masonry elements with mixtures that have higher aggregate content and partial cement replacement with limestone filler and metakaolin, achieving satisfactory results in buildability, mechanical strength, and efficiency.

Keywords: Aggregate; Supplementary materials; Construction efficiency; 3DCP Structural masonry; Sustainability.

Resumen: El presente estudio tiene como objetivo ampliar el conocimiento sobre mezclas cementosas con bajo contenido de cemento y altos niveles de adiciones minerales y agregados, evaluando su influencia en las propiedades constructivas de elementos impresos representativos de mampostería estructural. Se definieron parámetros y geometrías de impresión que permiten crear estructuras autoportantes, buscando hacer el proceso de construcción más rápido, eficiente y sencillo. En estado endurecido se analizaron la absorción de agua, la resistencia a la compresión y a la flexión en piezas pequeñas, así como la resistencia a la compresión de los bloques 3DCP y la adherencia entre capas. Los resultados obtenidos demuestran que, con los parámetros adoptados en el sistema de impresión utilizado, es posible producir elementos volumétricos de mampostería mediante mezclas con mayor contenido de áridos y sustitución parcial del cemento por masilla caliza y metacaolín, logrando resultados satisfactorios en edificabilidad, resistencia mecánica y eficiencia constructiva.

Palabras clave: Agregado; Materiales suplementarios; Eficiencia de la construcción; Albañilería estructural 3DCP; Sostenibilidad.

Received: 02-03-2025 / **Accepted**: 01-12-2025 / **Published**: 29-06-2026

Citation: Nascimento RF, Anjos MAS, Nascimento Júnior JP, Pessoa LR, Dias LS. 2026. Mechanical characterisation of 3D printed concrete masonry units with high aggregate and mineral addition content. *Mater. Construcc*. 76(361):e401. https://doi.org/10.3989/mc.2026.412825

Supplementary information ↓

1. INTRODUCTION

Additive manufacturing has been gaining traction across various industrial sectors, including construction. As a result, houses, bridges, and other types of structures have been built using 3D printing technology. This technique involves the extrusion of cementitious material by a gantry or robotic arm printer with an attached nozzle, constructing elements through layer-by-layer deposition based on the modeling of the element using computer-aided design (1-4).

Compared to the conventional molding method for cementitious materials, 3D printing of concrete or mortar (3DCP) offers several economic and environmental advantages, including architectural freedom for the fabrication of non-linear structures; fast construction speed; low labor requirements; reduced production costs due to decreased material volume and the elimination of formwork; waste reduction; improved efficiency; and increased productivity (5- 8).

A crucial aspect of 3D printing with extrusion technology is formulating an appropriate cementitious mixture that meets sustainability criteria. Initially, materials used for 3D printing were high-performance concretes with a high cement content, which has a notably negative environmental impact (6). For this reason, efforts have been made to reduce cement consumption in these mixtures by incorporating supplementary materials that can partially replace cement while maintaining similar characteristics to the mixtures. Materials such as silica fume, fly ash, metakaolin, and limestone filler have shown satisfactory responses for use in 3D Concrete Printing (3DCP) (9).

In addition to using supplementary materials, another option for further reducing cement consumption is increasing the aggregate content in the mixture. The most commonly used aggregate in construction and 3DCP is sand, which, according to He *et al.* (10), is essential for the solid-liquid biphasic system of mortars. The main advantages of using sand, aside from reducing binder consumption, include reducing shrinkage, volumetric variation, and crack formation, ensuring material durability. The characteristics of sand, particularly morphology, size, origin, and grading, influence the properties of the mortar (11). In 3DCP printing, these factors become even more significant, as the aggregate content, particle size distribution, and type of aggregate, combined with the paste's rheology, play a crucial role in determining the viscosity and yield stress of the 3DCP mixture (12).

The selection of materials for a 3DCP mixture project must ensure pumpability, extrudability, printability and constructability (13) while also promoting greater sustainability to ensure the integrity and durability of constructions through additive manufacturing. Zhang *et al.* (14) found that cementitious mixtures with better thixotropic properties have higher initial flow for pumping and better resistance to deformation after extrusion. This thixotropic rheological behavior is mainly achieved by the addition of additives and viscosity-modifying agents, as well as the use of supplementary cementitious materials such as fly ash, silica fume, and metakaolin (15).

Metakaolin (MK) is a pozzolanic material that, when it reacts with calcium hydroxide and water, results in the formation of calcium aluminosilicate hydrates (C-A-S-H), promoting the enhancement of mechanical properties (16). The main effect of metakaolin in a cementitious mixture is the reduction of workability due to its high specific surface area, which requires higher water content and superplasticizer (17). Therefore, using more than 10% metakaolin results in high shear strength and may cause difficulties in extrusion and reduce the open time of the 3DCP mixture (18). The advantage of using metakaolin in appropriate proportions lies in its ability to create a strong interconnected network in the cement paste, improving the structural stability of the printed element.

Limestone filler (LF), although not a pozzolan, plays an important role in partially replacing Portland cement, as it produces a greater volume of paste in the mixture. Additionally, its morphological characteristics influence the improvement of workability due to its rounded particles (19, 20) and the filling of voids in a packing process that makes the mixture denser (21).

The combined effect of metakaolin and limestone filler has proven to be satisfactory in reducing the cement consumption of 3DCP mixtures, as demonstrated by Barbosa *et al.* (22) and Nunes *et al.* (23), who reduced cement use from 706 kg/m³ to 406 kg/m³. From 687 kg/m³ to 338 kg/m³, respectively, while maintaining good construction capacity.

In the context of 3D printing, besides aiming to develop sustainable mixtures with adequate quality and printability, attention must also be given to the mechanical behavior of the elements, especially considering the application of the mixtures in masonry construction. Thus, for the evaluation of a printed element, ISO/ASTM 52939 (24) suggests that a model of a complex part of the element to be 3D printed should be built to demonstrate that the element is printable and achieves the required shape within the allowed tolerances and those outlined in the digital model. Furthermore, the produced samples can be used to derive statements about the expected mechanical and technological properties.

Thus, studies have been conducted to understand the behavior of large-scale elements, such as those developed by Han *et al.* (25), Daungwilailuk, Pheinsusom, and Pansuk (26), Nunes *et al.* (23), and Anjos *et al.* (27). Han *et al.* (25) emphasized the application of 3DCP with geometry containing an internal W-type truss and reinforcement. Daungwilailuk, Pheinsusom, and Pansuk (26) evaluated the capacity of 3DCP walls as structural elements, considering a wall with a flat geometry of 120 x 1320 x 77 mm (width, length, and height, respectively) containing internal trusses. Nunes *et al.* (23) evaluated the mechanical behavior of mixtures in representative volumetric element of 3DCP masonry (RVE-3DCP) with internal truss geometry. Anjos *et al.* (27) evaluated RVE-3DCP with different typologies. Nunes *et al.* (23) and Anjos *et al.* (27) address the sustainable nature of the materials used for printing in their research. However, their cement consumption is still higher than what is intended in this research.

In this context, considering the limited number of studies on representative volumetric masonry elements using low-cement-content mixtures and without internal truss geometry, the main objective of this study is to evaluate properties related to printability and mechanical strength of mixtures with cement consumption of up to 20.72 kg/m². These mixtures are intended for the printing of large-scale elements without internal trusses, aiming to simplify and accelerate the printing process. This research seeks to contribute to sustainability-related aspects and to the advancement of the printing process with the proposed geometry, as most existing studies incorporate internal reinforcement or interlocking features in their evaluations. The properties assessed in the fresh and hardened states aim to characterize the mixtures and understand their behavior in practical applications for 3D-printed structural masonry.

2. MATERIALS

For the production of concrete mixtures intended for 3D printing, high early strength cement (CPV-ARI, a cement similar to CEM I), commercial metakaolin, limestone filler (with particles smaller than 74 µm), natural river sand, and chemical admixtures such as polycarboxylate-based superplasticizer and hydroxypropyl methylcellulose-based viscosity modifier were used. From a physical standpoint, the materials exhibit characteristics that contribute to the behavior of the mixture in the fresh state (Table 1). The CPV-ARI cement has the highest bulk density among the solid components, with a value of 3.13 g/cm³, which is related to its high calcium oxide content. The limestone filler, in turn, presents an intermediate density of 2.88 g/cm³, while the metakaolin, with a density of 2.53 g/cm³, stands out for its high specific surface area (23.00 m²/g), indicating the presence of extremely fine and reactive particles. This characteristic gives metakaolin an important role in modifying the mixture's viscosity and pozzolanic activity, promoting secondary reactions that contribute to long-term strength gain.

The river sand used has a bulk density of 2.49 g/cm³ and consists of particles with a maximum diameter of 2.36 mm. It contains 3.34% fine material and has a fineness modulus of 1.79, being classified as a relatively fine sand. These characteristics are suitable for 3D printing, as they allow good resolution and finish of the extruded layers, as well as favoring the cohesion and workability of the mixture.

Table 1. Physical characterization of materials.

Material	Bulk density (g/cm³)	Average diameter (µm)	Surface area BET (m²/g)	Maximum diameter (mm)	Powdery material content (%)	Fineness Modulus
Sand	2.49	-	-	2.36	3.34	1.79
CPV - ARI	3.13	8.51	1.70	-	-	-
Metakaolin	2.53	11.77	23.00			
Limestone filler	2.88	11.91	2.75			

Regarding the particle size distribution of the materials (Figure 1), it is observed that the cement has finer particles (average diameter of 8.51 µm), while the limestone filler and metakaolin have slightly coarser particles, with average diameters of 11.91 µm and 11.77 µm, respectively. However, metakaolin stands out due to a broader distribution of fine particles, which is reflected in its high specific surface area. This difference has important implications for the material's rheology, since fine particles increase water demand and can raise the mixture's viscosity, requiring greater control with admixtures.

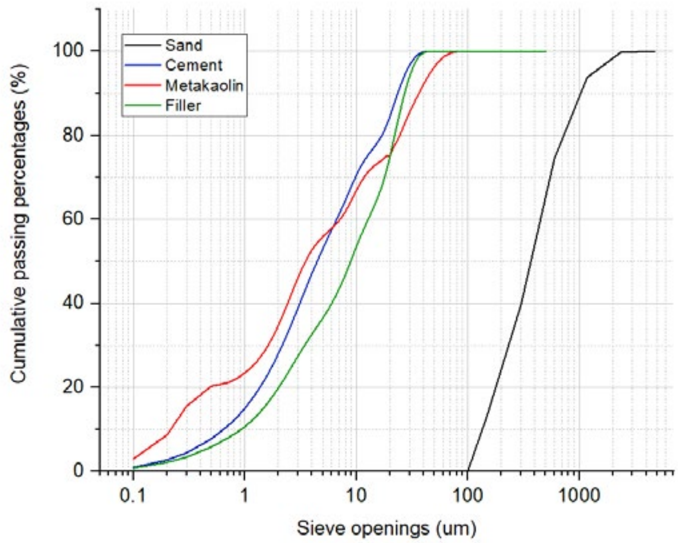

Figure 1. Particle size distribution of the materials.

From a chemical standpoint (Table 2), each material contributes differently to the hydration reactions and the formation of the concrete microstructure. CPV-ARI cement exhibits a typical Portland cement composition, with a high calcium oxide (CaO) content corresponding to 77.29% of its composition. Silicon oxide (SiO_2 – 11.10%), sulfur (SO_3 – 4.72%), and iron oxide (Fe_2O_3 – 3.86%) are also present, actively participating in the hydration process and the formation of cementitious products. Metakaolin, a pozzolanic material, is characterized by high contents of silicon oxide (SiO_2 – 56.80%) and aluminum oxide (Al_2O_3 – 26.30%), which react with cement hydration products, such as calcium hydroxide, forming additional cementitious compounds like calcium silicate hydrate (C-S-H).

Limestone filler is mainly composed of calcium oxide (CaO – 91.22%), with smaller amounts of magnesium oxide (MgO – 4.69%) and silica (SiO_2 – 3.41%). Its primary function is physical, acting as a filler material and contributing to improved cohesion between layers and greater dimensional stability of the printed mixture. Chemically, limestone filler can act as a nucleation agent, accelerating the onset of cement hydration and aiding in rheology control.

Thus, the combination of these materials, with different physical and chemical properties, allows the mixture to be adjusted to meet the specific requirements of 3D printing, such as extrudability, shape stability, interlayer adhesion, and mechanical strength. The use of appropriate chemical admixtures complements this balance, enabling the system to perform adequately in both the fresh and hardened states.

Table 2. Chemical Characterization of Materials.

	SiO_2	Al_2O_3	Fe_2O_3	K_2O	CaO	MgO	SO_3	TiO_2	Others*
LF	3.413	-	0.468	0.073	91.216	4.692	-	-	0.138
MK	57.795	27.302	5.477	3.396	0.831	-	0.161	3.775	1.263
CPV – ARI	11.095	0.459	3.859	1.730	77.290	-	4.718	0.341	0.508

*Sum of oxides with a content of < 2,0% in all precursors, simultaneously.

3. DEFINITION OF THE MIXTURES AND PRINTING PROCEDURES

The analyzed mixtures were divided into two groups with reference compositions of 1:2 (cement:sand) and 1:3 (cement:sand), chosen based on previous work from the research group of the authors Barbosa *et al.* (22), Nunes *et al.* (23), and Dias *et al.* (28). The mixture with a higher aggregate content (1:3) did not show the ability to construct with the printing system used by these authors, which had different printing parameters compared to those used in the present study, including nozzle diameter, deposition height, extrusion speed, pumping rate, and flow rate. It is known, however, that the printing and pumping capacity depends on the available systems, and thus mixtures compatible with these systems are defined.

Therefore, cementitious mixtures were analyzed for the same printing system as in the previous studies by Barbosa *et al.* (22), Nunes *et al.* (23), and Dias *et al.* (28). However, different parameters were applied, as presented in Table 2, to enable the printing of mixtures with higher aggregate content and lower cement consumption, as shown in Table 3, which presents the material consumption for producing one square meter of masonry in the proposed construction typology. The aim is to analyze the influence of aggregate content and mineral additions on the fresh and hardened behavior of 3DCP mixtures printed in smaller-scale models of the element to be printed (masonry).

The proposed methodology was to identify printable mixtures under the conditions of the printing system and then reduce the cement consumption of the mixtures while maintaining constant Vp/Vs ratios (Paste volume/Aggregate volume) in the 1:2 and 1:3 compositions, as shown in the flowchart in Figure 2.

Table 3. Printing parameters.

Parameter	Dimension
Nozzle diameter	40 mm
Deposition height	20 mm
Printing speed	2000 mm/min
Extrusion speed	34 – 46 rpm
Extrusion frequency	18 – 24 Hz
Extrusion rate	35 – 45 ml/s

Table 4. Material consumption in kg/m² of masonry.

Mixture	CP (kg/m²)	LF (kg/m²)	MK (kg/m²)	S	Water (kg/m²)	SP (kg/m²)	Water/ cement - a/c	a/mf*	a/ms**	%SP	HPMC (kg/m²)
12REF	70.79			(kg/m²)	25.49	0.28	0.36	0.36	0.12	0.4	0.11
12MLF40	34.95	27.96	6.99	141.59	25.16	0.49	0.72	0.36	0.12	0.7	0.10
12MLC50	27.91	34.89	6.98	139.81	25.12	0.49	0.90	0.36	0.12	0.7	0.10
13REF	52.36			139.54	25.14	0.16	0.48	0.48	0.12	0.3	0.08
13MLF40	25.94	20.75	5.19	157.09	24.90	0.31	0.96	0.48	0.12	0.6	0.08
13MLF50	20.72	25.90	5.18	155.63	24.87	0.31	1.20	0.48	0.12	0.6	0.08

* a/mf = water/fine materials ratio (mf = CP + MK + FC); ** a/ms = water/dry materials ratio (ms = CP + MK + FC + S).

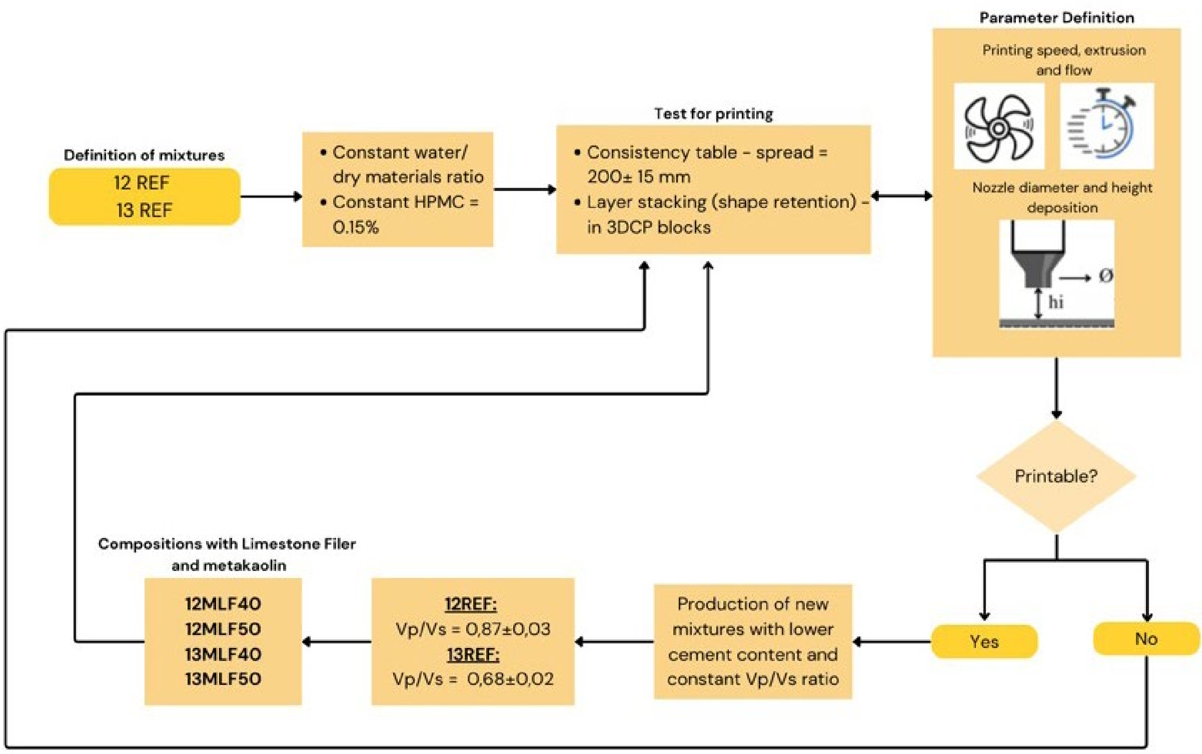

Figure 2. Flowchart for mixture definition.

The mixtures had a constant water/dry materials ratio (a/ms) of 12%, which was necessary for the proper wetting of the materials. The proportion of HPMC used was fixed at 0.15% relative to the mass of the cementitious materials. The superplasticizer content was adjusted according to the demands of each mixture, with the goal of maintaining similar rheological characteristics among them and ensuring printability and extrusion capacity with the same pumping conditions, speed, and printing volume.

The properties used to define the superplasticizer content in the mixtures were the mortar spread on the consistency table (29) and layer stacking (shape retention) (28), which provide important information regarding the consistency, extrusion, and printability of the material.

For the printing system used, the mixtures should present a spread on the consistency table of 200 ± 15 mm to ensure adequate pumping and printing capacity. Based on this, printing parameters such as speed and extrusion rate are adjusted for each mixture to achieve printability of the layer without surface defects, including any discontinuities due to excessive rigidity and inadequate cohesion between successive layers (24).

The tests to define the superplasticizer content were initially conducted on the reference mixtures (12REF and 13REF) until adequate consistency for extrusion and printability was achieved. Once it was verified that the mixtures were printable with a specific superplasticizer content, the next step was to produce new mixtures with reduced cement consumption, using limestone filler and metakaolin as partial substitutes for the binder while keeping the Vp/Vs ratios constant. For the mixtures with substitutions, the same procedure was followed to determine the superplasticizer content.

For the printing process, a 3D printer for mortar, concrete, and soil was used, structured in a gantry configuration with dimensions of 1000 mm x 1000 mm x 1500 mm (X, Y, and Z axes), featuring an extrusion system with a 40 mm diameter circular nozzle (Figure 3). Additionally, all mixtures were produced using an inclined-axis mixer, following this sequence: homogenization of dry materials (cement and sand), introduction of 80% of the mixing water, incorporation of the superplasticizer, addition of the remaining 20% of water, the introduction of limestone filler, addition of metakaolin, and finally, incorporation of the HPMC additive. It is important to note that each step of the mixing process was subjected to a duration of 2 minutes.

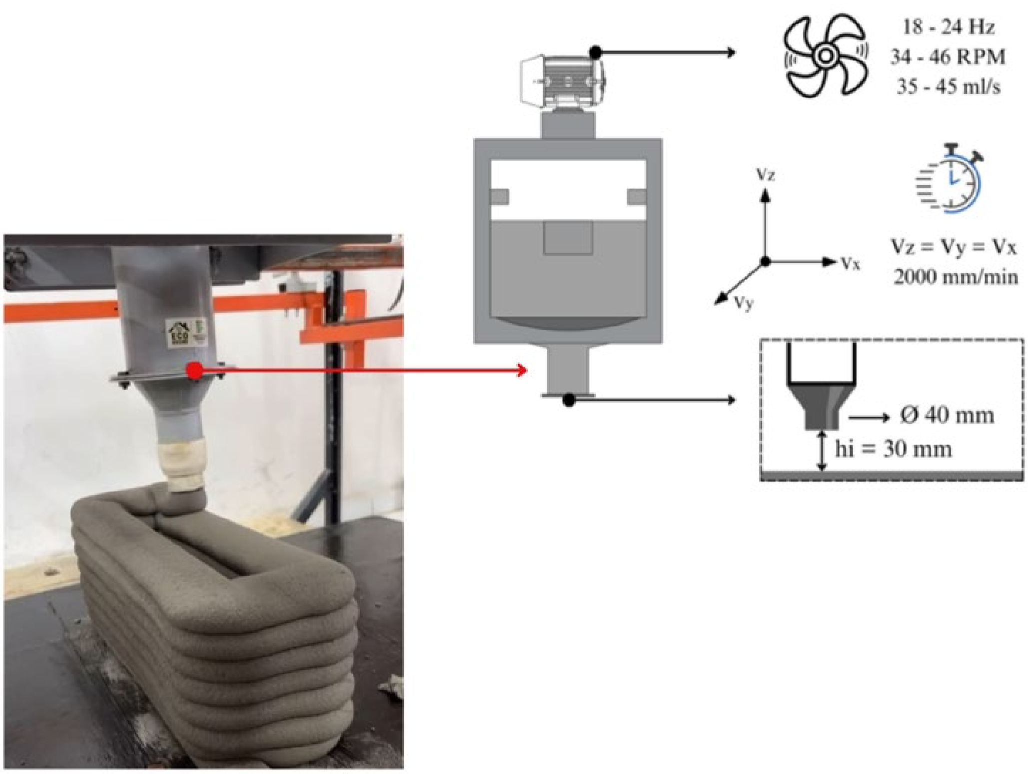

Figure 3. Printer and printing parameters.

According to ISO/ASTM 52939 (24), the evaluation of properties for 3D printed masonry should include the following steps: 1. Project definition; 2. Printing of the element; 3. Verification of mechanical properties. As defined in Table A.2 of the aforementioned standard, the mechanical verification step recommends that tests be conducted on masonry elements such as prisms. Before this geometry, compressive strength tests can be performed on 3DCP blocks.

Since the focus of the proposed application is masonry construction, it was decided that the printed piece would be a volumetric element representative of masonry, referred to in this study as a 3DCP block, with project dimensions of 150 x 200 x 400 mm (width, height, and length, respectively), and its schematic model can be seen in Figure 4. As presented, the block has no septum or internal locking, so the interior of the block is hollow. This geometry allows, for example, the placement of insulating material inside the empty space. Four blocks were made for each composition for the compression strength test, totaling 24 blocks.

Additionally, the use of the 40 mm diameter nozzle aimed to produce a filament thickness of 50±5 mm. With this filament thickness, it is possible to increase the layer height while maintaining stability and shape retention. The digital model specifies that the height of each layer should be 20 mm ± 0.5 mm; thus, for a block with a height of 200 mm, 10 layers are required.

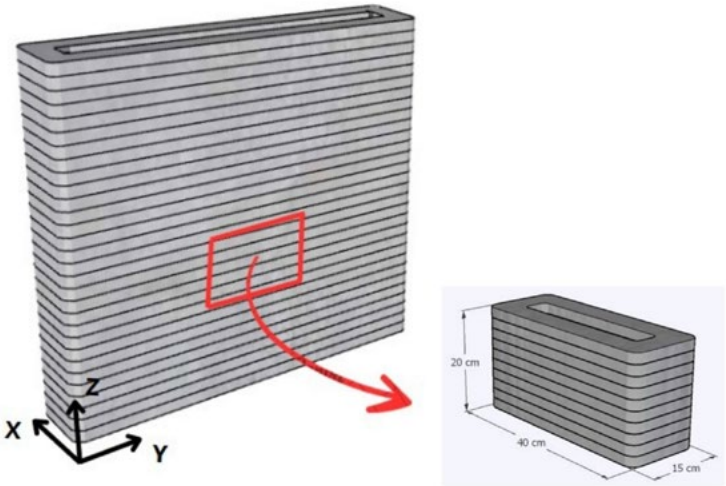

Figure 4. 3DCP block geometry.

3DCP blocks were also printed to extract prisms with dimensions of 40 x 40 x 160 mm to evaluate mechanical properties in small specimens in two directions (X and Y), as well as total water absorption and physical indices. The extraction of the prismatic test specimens was performed in the hardened state with the aid of a machine equipped with a diamond-cutting disc, as shown in the schematic presented in Figure 5. One block was produced for each mixture to extract four specimens for each test, totaling 72 test specimens. These were subjected to wet curing for 28 days, and testing procedures were carried out after this period.

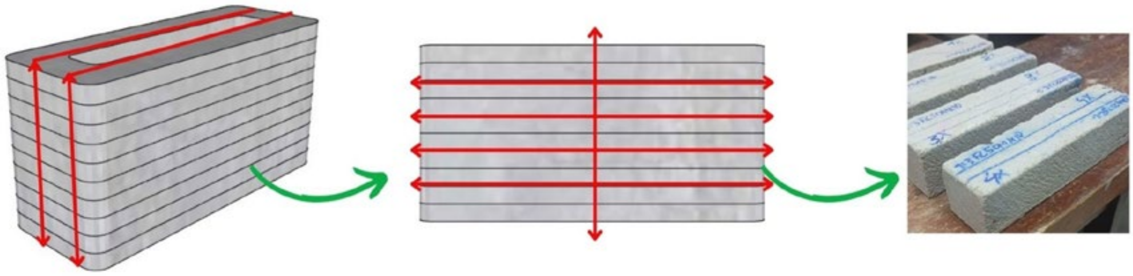

Figure 5. Cutting scheme of the 3DCP blocks for obtaining the prisms.

4. FRESH STATE TESTS

4.1. Verification of printing requirements

ISO/ASTM 52939 (24) suggests carrying out viability verification and qualification steps as a prerequisite for mass production through additive manufacturing. This verification consists of steps that involve design, the 3D printing process, dimensional and tolerance verification, and properties of the printed materials. In this study, the printing verification was conducted by comparing the dimensions designed in the digital model with the actual dimensions obtained after the printing process, through measurements taken from four blocks of each composition. A visual inspection of the printed layer was also performed using images to evaluate surface defects, including any discontinuities due to excessive rigidity and inadequate cohesion between successive layers.

4.2. Bulk density and incorporated air content

The incorporated air content in the mixture affects the mechanical properties of the cementitious composite and also impacts its bulk density. Therefore, these properties were characterized based on NBR 13278 (30).

4.3. Green compressive strength test

Green compressive strength is a strength test performed on the material while it is still fresh, checking how much load it can withstand in the initial stages. This test is essential to determine the initial deformation of each mixture and, therefore, to determine how many layers can be stacked without excessive deformation, especially when considering a masonry printing context. Thus, the test is associated with the element's construction capacity.

To evaluate the green compressive strength of the mixtures during the printing process, a sample with a length of 100 mm and consisting of three printed layers (Figure 6a), produced under the same conditions as the 3DCP blocks, is subjected to loading at a constant speed of 0.1 mm/s, with real-time load readings taken. During the test, load and displacement values are recorded at defined points on the sample according to the parameters established for the tests (Figure 6b). Measurements were taken at different time intervals: T0 (immediately after printing), T15 (15 minutes after printing), T30 (30 minutes after printing), and T60 (60 minutes); the tests were conducted in duplicate.

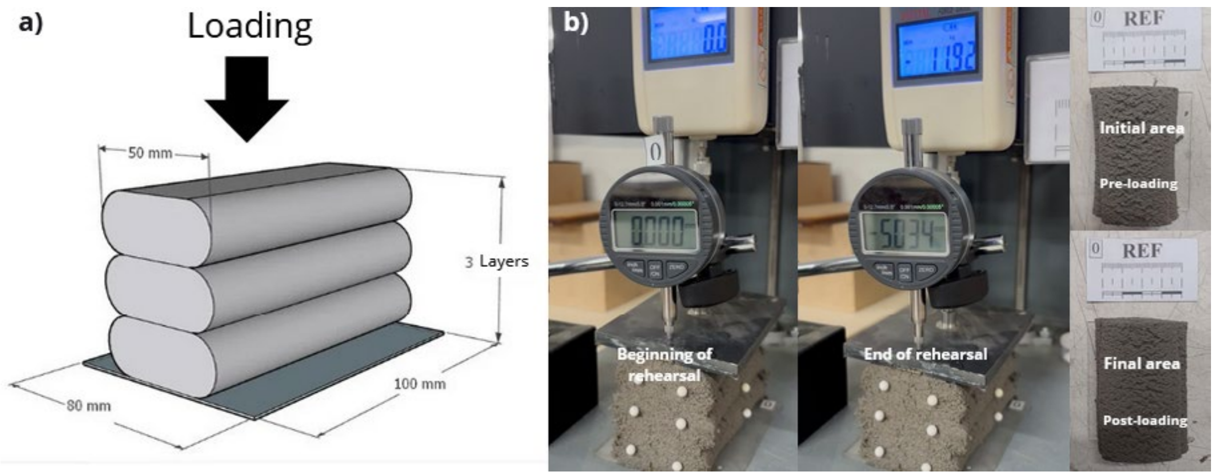

Figure 6. Green compressive strength test.

5. TESTS IN THE HARDENED STATE

5.1. Compressive strength of 3DCP blocks

The compressive strength test of the blocks was conducted in accordance with the guidelines established in NBR 12118 (31) on 4 3DCP blocks after 28 days of immersion curing in water. A press was used for the test with a loading rate of 0.05 MPa/s, as specified in the standard. The efficiency of the blocks is calculated by dividing the cement consumption (in kg/m²) of each mixture by its compressive strength. Therefore, the lower the value of this ratio, the better the block's efficiency, as less cement is needed to produce 1 MPa of strength.

5.2. Compressive and flexural strength of small 3DCP specimens

Since 3DCP exhibits anisotropy, meaning different strengths in each direction, after 28 days of immersion curing, 4 prismatic test specimens from each mixture were subjected to flexural testing. These specimens were extracted from the 3DCP block using a diamond-cutting disc machine with dimensions of 40 mm x 40 mm x 160 mm. The specimens were tested in the X direction (direction of height increase in the printed material) and the Y direction (perpendicular to the X and Z planes). The test was conducted in accordance with the NBR 13279 (32) standard using a Shimadzu® AG-X 10 kN universal testing machine with a loading rate of 50 N/s. Furthermore, after the flexural strength test, the specimens, divided into two parts, were used for the compressive strength test, as per NBR 13279 (32).

5.3. Adhesion between layers

The adhesion test between layers was carried out with the aim of determining the degree of connection between the layers, a fundamental characteristic for maintaining the physical integrity of the element as well as its resistance capacity.

To obtain the adhesion strength between layers, a 40 cm long piece was initially printed, consisting of two layers. Samples were extracted from this structure for the test. Both printed layers of the different specimens were prepared from the same batch of mixture. Regarding the dimensions of the tested samples, their length was 5 cm, while the height and width were determined by the natural deformations and spread of each mixture.

The adhesion between layers was determined based on the diametral compression tensile strength test (33) using the 3DCP test setup used in previous work (34, 35). The test was performed on 4 samples cut from the initial filament using a diamond-cutting disc after 1, 7, and 28 days of immersion curing.

The calculation of the adhesion strength between layers as a function of time was performed using Equation [1]:

$$Rad = \frac{2F}{\pi A} \qquad [1]$$

Where: *Rad* (MPa) is the adhesion strength between layers; F (N) is the ultimate applied load; and A (mm²) is the adhered interface area.

5.4. Water absorption, void index, and bulk density

The water absorption and void index test provides an idea of the compactness of the mixtures. Greater absorption is related to a greater number of voids, which indicates that the composition is less compact. This is reflected in the mechanical resistance, which tends to be lower the greater the number of voids.

For the evaluation of water absorption capacity and the determination of void index and bulk density, prismatic test specimens with dimensions of 40 mm x 40 mm x 160 mm were extracted from the 3DCP block. These specimens were subjected to the test established in NBR 9778 (36) at 28 days of age after immersion curing.

5.5. Capillary water absorption

The capillary water absorption test was conducted according to NBR 15259 (37) at 28 days of curing, using prismatic specimens extracted from the 3DCP block. The dry masses of the samples were determined, followed by immersion in a 5 mm water layer. The masses were then measured at 10 and 90 minutes of testing. Based on these values, the absorption at the respective times and the capillarity coefficient of the material were calculated.

6. RESULTS AND DISCUSSION

6.1. Verification of printing requirements

Table 4 presents the verification of the printing requirements by comparing the proposed 3D design with the actual printed object across the three dimensions of the 3DCP block. This is an important verification step, as referenced in ISO/ASTM 52939 (24), for checking the tolerances of the elements as part of quality control. The block dimensions varied by less than 5%, except for mixtures 13MLF40 and 13MLF50, which differed in width by 7% and 6%, respectively.

Figure 7 illustrates the visual assessment of the printing process. It reveals that mixture 13REF had defects due to lower cohesion and higher particle friction, resulting in a discontinuous appearance with more voids. The defects in the 13REF mix are related to the lower ratio between the volume of paste and the volume of aggregate (Vp/Vs) compared to the 1:2 series and the absence of LF and MK. Overall, the 1:2 series mixtures demonstrated a better surface finish and a more cohesive appearance during printing than the 1:3 series mixtures, a behavior attributed to the higher Vp/Vs ratio in the 1:2 series mixtures.

Table 5. Check of dimensions and tolerances.

	Designed length 40 cm		Designed width 15 cm		Designed height 20 cm	
Mixture	**Average Length (cm)**	**Designed vs. Printed Difference**	**Average Width (cm)**	**Designed vs. Printed Difference**	**Average Height (cm)**	**Designed vs. Printed Difference**
12REF	40.79	2%	15.63	4%	20.24	1%
12MLF40	40.78	2%	15.81	5%	19.84	-1%
12MLF50	40.33	1%	15.46	3%	19.77	-1%
13REF	40.96	2%	15.73	5%	20.03	0%
13MLF40	41.55	4%	15.99	7%	20.29	1%
13MLF50	40.93	2%	15.84	6%	20.18	1%

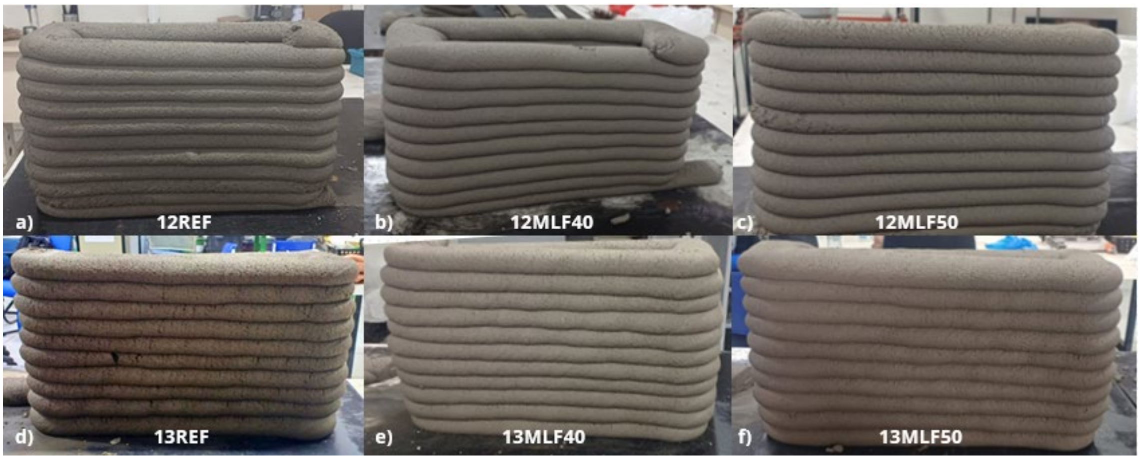

Figure 7. 3DCP blocks of each mixture.

6.2.Bulk density and incorporated air content

Figure 8 highlights the results for bulk density and incorporated air content. Within each group, the mixtures exhibited similar density values, indicating that the partial replacement of cement with limestone filler and metakaolin¬¬, despite their lower specific densities, did not significantly alter the mixtures' fresh-state densities.

However, when comparing the mixtures in the 1:2 series with those in the 1:3 series, a reduction in density values is noticeable for the latter group. This is due to the more significant amount of aggregate in the mix, which is lighter than the binder. In addition, as the grain size of sand is larger than that of the other materials, increasing the aggregate content creates more voids, reducing density unless the packing of the sand with the other materials is optimized.

The density values were lower than those obtained by Wolfs *et al.* (38) and Nunes *et al.* (23) for similar compositions, also indicating higher air incorporation in the mixtures. This can be explained by the type and morphology of the materials used, as well as the mixing processes adopted.

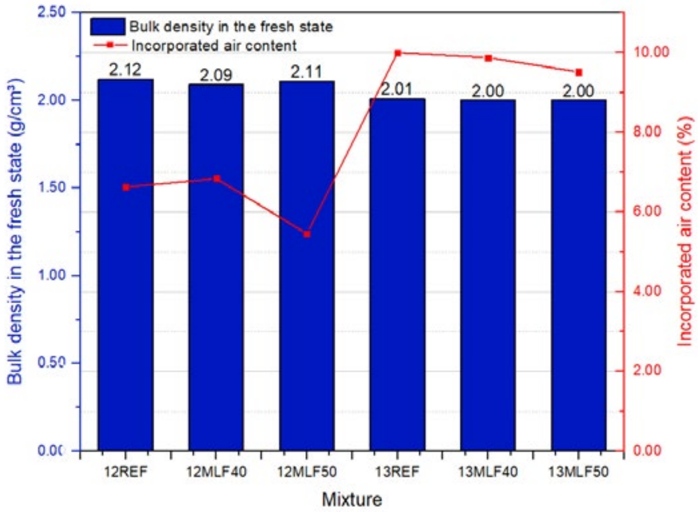

Figure 8. Bulk density and incorporated air content.

The 13REF mix has the highest incorporated air content (10.00%) due to its higher aggregate content and lower paste volume. When introducing limestone filler and metakaolin and increasing the volume of paste in the composition, there is a decrease in the value (9.88% - 13MLF40 and 9.52% - 13MLF50). This reduction occurs because the increased paste volume fills the voids between the aggregate particles more effectively, leading to less trapped air.

6.3. Green compressive strength test

Figure 9 shows the results of the green compressive strength test for each mixture at 0, 15, 30, and 60 minutes after filament printing. For the same applied stress level, the 1:2 series mixtures exhibit lower deformations. For constructing 1 m² of the proposed geometry, the stress for five layers is 0.0020 MPa, while for ten layers, it is 0.0040 MPa. Thus, printing is feasible from T0 in both cases, with deformations below 5%.

A 5% deformation at T0 and T15 requires stress between 0.005 MPa and 0.025 MPa, corresponding to approximately 25 to 60 stacked layers, depending on the mixture used. The 1:2 series mixtures are associated with more layers as they support higher stress levels. For a more significant number of layers, printing should be performed at T30 or T60 since the reduction in consistency over time results in lower deformations.

Panda, Lim, and Tan (39) also evaluated the relationship between deformation of fresh-state mixtures and the buildability of 3D printed materials, finding that the addition of nanoclay improves the mixture's thixotropy, allowing for maximized build height through increased stiffness and green strength. This indicates that the use of mineral additions in 3D printing mixtures can enhance the structuring and stability of the printed material, enabling the construction of greater heights with minimal deformation. In the absence of formwork, printable materials are expected to withstand the self-weight of the structure being printed in order to prevent plastic collapse and mitigate instability (40).

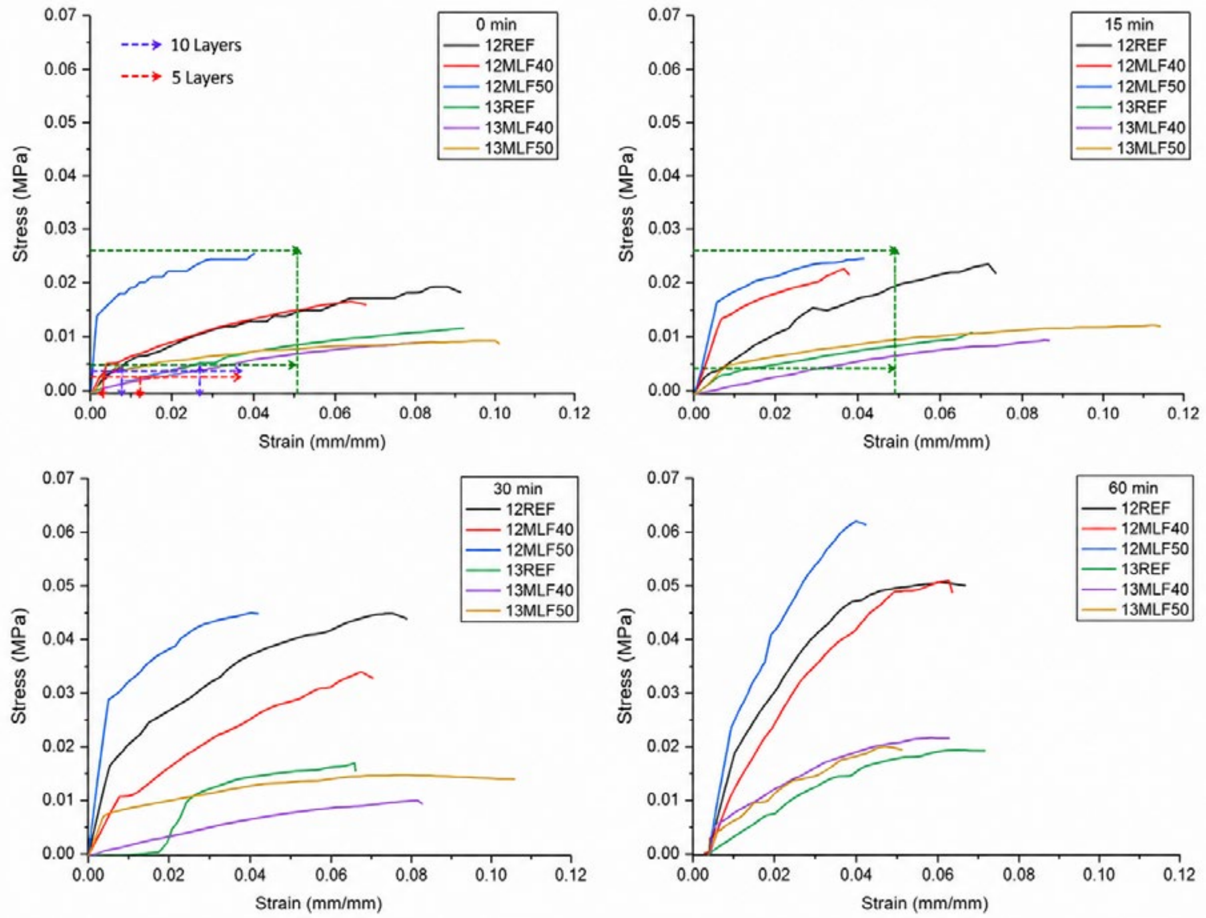

Figure 9. Stress x strain.

6.4. Total water absorption and void index

The 12REF and 13REF mixtures exhibit lower void volume and water absorption (Figure 10) due to their higher cement content and lower water-to-cement ratio than mixtures containing MK and LF. The higher absorption observed in the 13MLF40 and 13MLF50 compositions demonstrates that the increased filler content led to more voids in the hardened material due to the reduced volume of hydrated products, which would otherwise occupy space in the matrix.

Comparing the 1:2 and 1:3 mixture groups, the higher aggregate content increased void volume. This result is also due to the lower cement consumption and higher water-to-cement ratio, resulting in higher porosity, as was also verified by Dias *et al.* (28) reported that mixtures with higher aggregate content tend to exhibit greater interparticle porosity, especially in printing processes where mechanical compaction is absent. This results in higher void indices. These factors directly impact the strength of the mixtures.

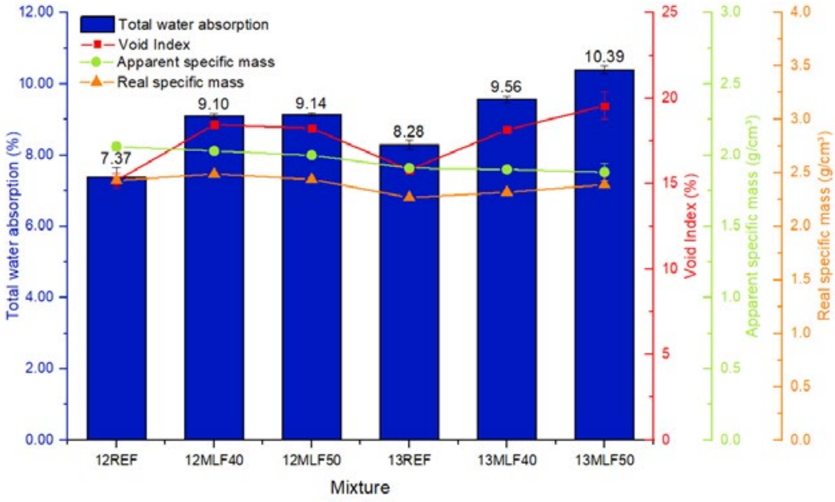

Figure 10. Total water absorption x void index x specific mass.

6.5. Water absorption by capillarity

Figure 11 illustrates the capillary absorption results at 10 and 90 minutes for each studied composition, along with their respective capillary coefficients. Incorporating limestone filler and metakaolin increased capillary absorption values due to the reduction in pore size caused by the partial replacement of cement with these materials.

Since the capillary cross-section is inversely proportional to the pore size, the smaller the radius of the capillaries, the higher the capillary absorption value (41). Furthermore, incorporating an extra 10% filler in the 12MLF50 and 13MLF50 mixes further increases the capillary section, emphasizing the filling effect of this mineral addition, particularly over time.

When comparing the two groups (1:2 and 1:3), the highest capillarity values are associated with the 1:3 series, influenced not only by the reduction in pore diameter but also by the greater overall porosity of the material due to the increase in aggregate content.

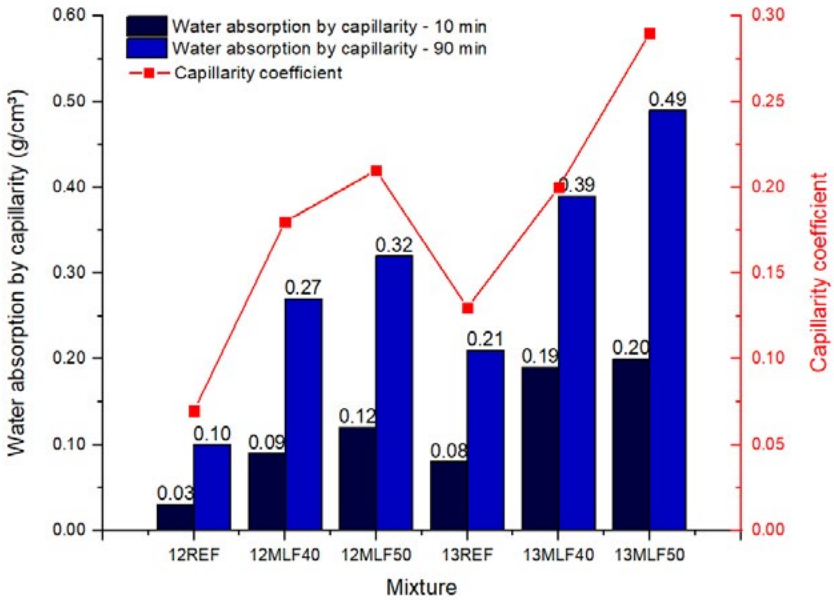

Figure 11. Absorption by capillarity.

Research involving 3D printed mixtures, especially those based on metakaolin, reveals that the porous structure of these materials tends to contain a higher proportion of fine pores. This favors water capillarity, despite the total porosity potentially being lower. A recent study by Jaji *et al.* (42) showed that, in 3D printed metakaolin-based geopolymers, capillary porosity tends to be predominant, while gel porosity decreases with curing time.

In the case of limestone filler, the literature also confirms its dual role: on one hand, it acts as a filler material, reducing larger voids between particles; on the other, it can increase capillary absorption when used in higher proportions, as it promotes the formation of smaller and more connected pores. Li *et al.* (43) demonstrated that the addition of up to 10% by mass of limestone filler in concretes contributed to microstructure densification, reducing total porosity and refining the pore distribution, which significantly decreased capillary absorption coefficients. However, at higher proportions, fine pores may facilitate capillary connectivity.

6.6. Compressive strength of 3DCP blocks

Figure 12 shows the compressive strength results of the 3DCP blocks for each mix and their efficiency in kilograms of cement per MPa produced (kg/m²/MPa). The 12REF composition exhibits the highest strength, with the highest cement consumption and the lowest water/cement ratio, resulting in lower porosity and more hydrated products that strengthen the cementitious material. Moreover, as the limestone filler content increases in the mixtures, the block's resistance decreases due to an increase in the void index, as seen in Figure 10.

The same behavior was observed by Chen *et al.* (44), Barbosa *et al.* (22), and Nunes *et al.* (23) and results from the dilution effect in hydration caused by the high filler content replacing cement, which reduces the volume of hydrated products and increases the material's porosity in the hardened state (18, 45). Accordingly, there is a reduction in strength of 27.71% and 46.96% for compositions 12MLF40 and 12MLF50, respectively, compared to reference 12REF and 34.19% and 30.98% in compositions 13MLF40 and 13MLF50, respectively, compared to 13REF reference.

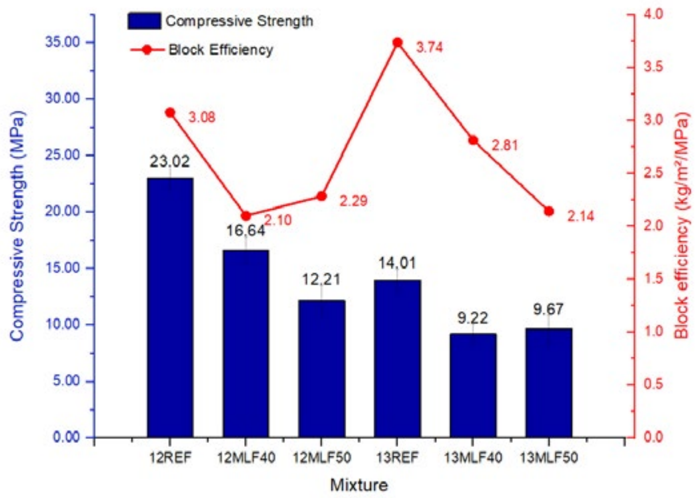

Figure 12. Compressive strength of 3DCP blocks.

The ANOVA statistical analysis (Table 5) with critical F < F and p-value < 5% shows that the strength values differ significantly. The Tukey test indicates that the strengths of the 3DCP blocks of the 12MLF40 and 12MLF50 compositions do not differ significantly from those of 13REF. This fact is noteworthy because, despite the higher cement consumption, the strength of the 13REF block can be compared to that of the 12MLF40 and 12MLF50 mixtures, with cement consumption 33.25% and 46.70% lower than 13REF, respectively.

Table 6. Statistical analysis between mixtures by Anova and Tukey Test (3DCP blocks).

ANOVA						
Source of variation	**SQ**	**gl**	**MQ**	**F**	**P-value**	**F critical**
Between groups	347.76	5	69.55	54.62	1.093E-08	2.958
Within the groups	17.83	14	1.27			
TUKEY TEST						
Group ratio	12REF	12MLF40	12MLF50	13REF	13MLF40	13MLF50
12REF		0.00027	3.3E-07	5.846E-06	1.411E-08	2.207E-08
12MLF40			0.00166	0.10420	6.965E-06	1.464E-05
12MLF50				0.34610	0.02109	0.05977
13REF					0.00080	0.00203
13MLF40						0.99130
13MLF50						

*p-value < 0,05

Similarly, the block strengths of the 12MLF50 and 13MLF50 mixtures can be compared statistically, as well as the 13MLF50 with 13MLF40. Thus, the results analyzed demonstrate that the 13MLF50 mixture, considering the reduced cement consumption (20.72 kg/m²) and the lower Vp/Vs ratio, presents better results from the point of view of the efficiency of the cement content in producing 1 MPa of strength. This indicates that it is possible to produce printed elements with a higher aggregate content and with the replacement of cement by mineral additions. In addition to maintaining adequate mechanical performance and printability for the required purpose, it contributes to environmental issues, since the production of 1 MPa of strength with a lower cement consumption implies a reduction in CO_2 emissions associated with clinker.

It is also worth emphasizing that the 3DCP blocks from all the analyzed mixes can be used for structural purposes, according to NBR 6136 (46), which classifies blocks with compressive strength ≥ 4.0 MPa as structural elements. Further analyses of the strength of printed walls are needed to establish correlations between the strength of the walls and representative wall elements (3DCP blocks) and to perform shear and flexural-compressive strength tests of the walls. The researchers are currently developing these studies.

6.7. Compressive and flexural strength of small 3DCP specimens

Figure 13 and Figure 14 display the flexural and compressive strength results for the small specimens, measured in the X and Y directions, for each evaluated mixture. When comparing the flexural strength values in both directions, it is clear that there was a slight variation in the results. However, the X direction (loading applied perpendicular to the printing direction) reaches values 2% to 7% higher than the Y direction (loading applied parallel to the printing direction). An exception can be noted in the 13MLF40 composition, which exhibited a 14% higher strength in the Y direction compared to the X direction. Regarding compression, the X direction achieves values 8% to 16% higher than the Y direction, except for the 12MLF50 and 13MLF40 mixtures, which demonstrated strengths 1% and 5% higher, respectively, in the Y direction than in the X direction.

Lim *et al.* (47) and Le *et al.* (48) emphasize that the strength losses observed in directions parallel to the printing are largely due to the discontinuity between layers and the microstructure resulting from the deposition process. The findings of the present study are consistent with these conclusions; however, the level of anisotropy identified was slightly lower than reported in previous works. This behavior may be partially attributed to the geometry of the specimens adopted in this research.

The width and height of the printed layers influence the strength of the small specimens, as evidenced by the small variation in results between the X and Y directions. In the X direction, the small specimens lack adjacent layers between them, while in the Y direction, the specimens consist of only two layers, which limits the accumulated effect of discontinuity between deposition interfaces. In other studies (49-51), bending and compression specimens form with adjacent layers and more than two superimposed layers, which affects anisotropy. Hence, evaluating the complex element representing the object intended for construction proves essential, as ISO/ASTM 52939 (24) suggested.

Naturally, the highest strength values correspond to the 1:2 group mixtures due to the higher cement consumption compared to the 1:3 group. However, comparing the 12MLF40, 12MLF50, 13MLF40, and 13MLF50 mixtures with their respective references reveals a reduction of approximately 20% to 30% in flexural strength. In compression, this reduction ranges from 10% to 40%. Additionally, increasing the filler content in the mixture by 10% causes only slight variations in the results, offering an advantage in reducing cement consumption.

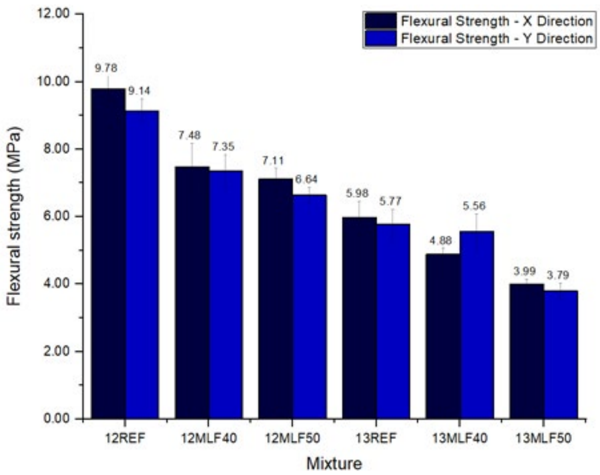

Figure 13. Flexural strength of small 3DCP pieces.

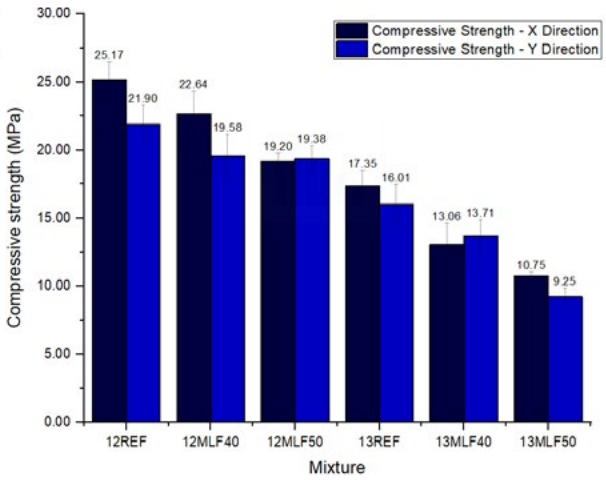

Figure 14. Compressive strength of small 3DCP pieces.

6.8. Adhesion between layers

Figure 15 provides the adhesion results between layers for each mix at 1, 7, and 28 days of curing is provided in Figure 15. As expected, the adhesion resistance values increase over time due to the formation of cement hydration products that enhance the material's densification and structuring. The 12REF mix shows the highest adhesion at all curing ages, which results from the higher cement consumption and the improved bond between the filaments (22, 52).

On the first day, the adhesion strength values of the 12MLF40 and 13REF compositions, as well as the 12MLF50, 13MLF40, and 13MLF50 mixtures, are close to each other, showing that despite the differences in the compositions, adhesion is not significantly affected by the variation in aggregate and mineral content at the initial stage. After 7 days, there is a greater distance between the curves until 28 days, when the differences between the compositions are more noticeable.

It is also observed that the adhesion strengths of the 12MLF40 and 13REF mixtures at 28 days have similar values, revealing that not only cement consumption is important to ensure good adhesion but also the volume of paste generated by the materials used in the mix.

The adhesion results indicate the need for analysis in larger pieces, as the 13REF, 12MLF40, and 12MLF50 mixtures show no statistical differences when analyzing the compressive strength of 3DCP blocks. However, differences appear in the adhesion between layers, which once again supports the guidance from ISO/ASTM 52939 (24) on the necessity of evaluating representative elements. In the case of adhesion between layers for printed parts, it seems essential to assess bending and shear strength in walls, as suggested by ISO/ASTM 52939 (24).

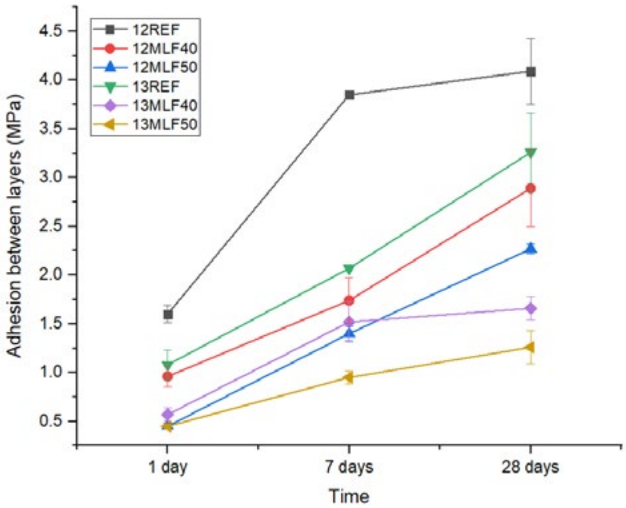

Figure 15. Adhesion between layers.

7. CONCLUSIONS

This study aimed to evaluate the behavior of mixtures in the fresh and hardened state with partial replacement of cement with limestone filler and metakaolin and variation in aggregate content for printing volumetric elements representative of a printed structural masonry - 3CDP blocks. The results are related to a system with specific parameters to achieve a faster printing process and a structure that supports itself without the need for internal locking. Therefore, it can be concluded that:

- The adopted printing parameters enabled the production of mixtures with a higher aggregate content than those traditionally used in 3DCP, and mineral additions such as limestone filler and metakaolin improved their printing quality.
- When comparing the 1:2 and 1:3 mix groups, the 1:3 group has a lower bulk density and an increase in the incorporated air content, given the higher aggregate content. The mixes with MK and LF have lower levels of entrapped air, demonstrating their ability to increase the paste content and improve the bonding between the material particles.
- The green compressive strength results show that, for $1m^2$ of the proposed geometry, printing 10 successive layers with less than 5% deformation is feasible, even at the initial time (T0). A 5% deformation corresponds to stress levels equivalent to various stacked layers, ranging from 25 to 60, depending on the composition used.
- Mixtures 12REF and 13REF have lower void volume and lower water absorption. The higher aggregate content contributed to increased absorption and volume of voids in the material, as evidenced by the lower apparent specific masses.
- The incorporation of limestone filler and metakaolin increased capillary absorption values due to the reduction in pore size provided by introducing these materials as a partial replacement for cement.
- The statistical analysis showed that the compressive strengths of the 3DCP blocks of the 12MLF40 and 12MLF50 compositions did not differ from the 13REF mixture, resulting in a 33% and 47% reduction in cement consumption for the same block strength.
- For most mixtures in the small specimens, flexural and compressive strength results showed slight variation in the X and Y directions. This variation is related to the width and height of the printed layers and the fact that the specimens in the X-direction had no adjacent layers, while those in the Y-direction consisted of only two layers.
- The results of adhesion between layers showed that the bond between layers is directly

related to the cement consumption and paste volume of the mixtures, so that the composition 13MLF50 has the lowest resistance to adhesion among the evaluated mixes.

Some considerations for future research include the need for strength analyses of full-scale printed walls to establish correlations between the strength of the walls and representative elements (3DCP blocks) and analyses of shear, bending, and compression resistance in walls.

Supplementary information ↑

Funding sources

Not applicable.

Supplementary material

Not applicable.

Data availability

Not applicable.

Acknowledgements

The authors thank CNPQ, CAPES, IFPB and FAPESQ-PB for the financial support given to the Project.

Authorship contribution statement

Raquel F. Nascimento: Formal Analysis, Data Curation, Investigation; Methodology, Project Administration, Writing – Original Draft, Writing – Review & Editing.

Marcos A. S. Anjos: Conceptualization, Supervision, Funding Acquisition, Investigation; Methodology, Data Curation, Formal Analysis, Project Administration, Writing – Original Draft, Writing – Review & Editing.

Josivan P. Nascimento Júnior: Data Curation, Writing – Review & Editing.

Leyla R. Pessoa: Data Curation, Writing – Review & Editing.

Leonardo S. Dias: Data Curation, Writing – Review & Editing.

Competing interests

The authors declare that they have no known competing financial interests or personal relationships that could have appeared to influence the work reported in this paper.

Statement on the use of Artificial Intelligence

Not applicable.

REFERENCES

1. Olsson NOE, Arica E, Woods R, Alonso J. 2021. Industry 4.0 in a project context: introducing 3D printing in construction projects. Proj. Leadersh. Soc. 2:100033. https://doi.org/10.1016/j.plas.2021.100033

2. Li LG, Xiao BF, Fang ZQ, Xiong Z, Chu SH, Kwan AKH. 2021. Feasibility of glass/basalt fiber reinforced seawater coral sand mortar for 3D printing. Addit. Manuf. 37:101684. https://doi.org/10.1016/j.addma.2020.101684

3. Shahmirzadi MR, Gholampour A, Kashani A, Ngo TD. 2021. Shrinkage behavior of cementitious 3D printing materials: effect of temperature and relative humidity. Cem. Concr. Compos. 124:104238. https://doi.org/10.1016/j.cemconcomp.2021.104238

4. Buswell RA, Leal de Silva WR, Jones SZ, Dirrenberger J. 2018. 3D printing using concrete extrusion: a roadmap for research. Cem. Concr. Res. 112:37–49. https://doi.org/10.1016/j.cemconres.2018.05.006

5. Ilcan H, Şahin O, Kul A, Yıldırım G, Şahmaran M. 2022. Rheological properties and compressive strength of construction and demolition waste-based geopolymer mortars for 3D printing. Constr. Build. Mater. 328:127114. https://doi.org/10.1016/j.conbuildmat.2022.127114

6. Skibicki S, Pułtorak M, Kaszyńska M, Hoffmann M, Ekiert E, Sibera D. 2022. The effect of using recycled PET aggregates on mechanical and durability properties of 3D printed mortar. Constr. Build. Mater. 335:127443. https://doi.org/10.1016/j.conbuildmat.2022.127443

7. Villaquirán-Caicedo MA, Fernández-González A, Fernández-García DA, Mejía de Gutiérrez R. 2023. Valorization of a low-quality coal ash, in the preparation of alkali activated inks for applications in 3D additive manufacturing. Constr. Build. Mater. 399:132598. https://doi.org/10.1016/j.conbuildmat.2023.132598

8. Dams B, Chen B, Kaya YF, Orr L, Kocer BB, Shepherd P, Kovac M, Ball RJ. 2024. Fresh properties and autonomous deposition of pseudoplastic cementitious mortars for aerial additive manufacturing. IEEE Access. 12:34606–34631. https://doi.org/10.1109/ACCESS.2024.3373188

9. Lu B, Weng Y, Li M, Qian Y, Leong KF, Tan MJ, Qian S. 2019. A systematical review of 3D printable cementitious materials. Constr. Build. Mater. 207:477–490. https://doi.org/10.1016/j.conbuildmat.2019.02.144

10. He XB, Fang YK, Peng Y, Shen W, Qiao D, Wang M. 2022. Mortar's rheological property and workability investigation based on morphology impact factor for graded sand particles. Constr. Build. Mater. 328:126987. https://doi.org/10.1016/j.conbuildmat.2022.126987

11. Li T, Nogueira R, de Brito J, Liu J. 2023. Influence of fine aggregate's morphology on mortars' rheology. J. Build. Eng. 63:105450. https://doi.org/10.1016/j.jobe.2022.105450

12. Kamakshi TA, Thakur MS, Subramaniam KV. 2024. Formulating printable concrete mixtures based on paste rheology and aggregate content: application to alkali-activated binders. Cem. Concr. Res. 184:107611. https://doi.org/10.1016/j.cemconres.2024.107611

13. Sotorrío G, Alonso J, Olsson NOE, Tenorio JA. 2021. Printability of materials for extrusion 3D printing technologies: a review of material requirements and testing. Mater. Construcc. 71(344):e267. https://doi.org/10.3989/mc.2021.11821

14. Zhang Y, Zhang YS, Liu G, Yang YG, Wu M, Pang B. 2018. Fresh properties of a novel 3D printing concrete ink. Constr. Build. Mater. 174:263–271. https://doi.org/10.1016/j.conbuildmat.2018.04.115

15. Bayat H, Kashani A. 2023. Analysis of rheological properties and printability of a 3D printing mortar containing silica fume, hydrated lime, and blast furnace slag. Mater. Today Commun. 37:107128. https://doi.org/10.1016/j.mtcomm.2023.107128

16. Provis JL, Duxson P, Van Deventer JSJ. 2010. The role of particle technology in developing sustainable construction materials. Adv. Powder Technol. 21(1):2-7. https://doi.org/10.1016/j.apt.2009.10.006

17. Homayoonmehr R, Ramezanianpour AA, Mirdarsoltany M. 2021. Influence of metakaolin on fresh properties, mechanical properties and corrosion resistance of concrete and its sustainability issues: a review. J. Build. Eng. 44:103011. https://doi.org/10.1016/j.jobe.2021.103011

18. Chen Y, Li Z, Chaves Figueiredo S, Çopuroğlu O, Veer F, Schlangen E. 2019. Limestone and Calcined Clay Based Sustainable Cementitious Materials for 3D Concrete Printing: A Fundamental Study of Extrudability and Early Age Strength Development. Appl. Sci. 9(9):1809. https://doi.org/10.3390/app9091809

19. Muzenda TR, Hou P, Kawashima S, Sui T, Cheng X. 2020. The role of limestone and calcined clay on the rheological properties of LC3. Cem. Concr. Compos. 107:103516. https://doi.org/10.1016/j.cemconcomp.2020.103516

20. Rojo López G, González Fonteboa B, Martínez Abella F, González Taboada I. 2022. Rheology, durability, and mechanical performance of sustainable self compacting concrete with metakaolin and limestone filler. Case Stud. Constr. Mater. 17:e01143. https://doi.org/10.1016/j.cscm.2022.e01143

21. Harbouz I, Rozière E, Yahia A, Loukili A. 2022. Printability assessment of cement based materials based on rheology, hydration kinetics, and viscoelastic properties. Constr. Build. Mater. 325:126810. https://doi.org/10.1016/j.conbuildmat.2022.126810

22. Barbosa MS, Anjos MAS, Cabral KC, Dias LS. 2022. Development of composites for 3D printing with reduced cement consumption. Constr. Build. Mater. 341:127775. https://doi.org/10.1016/j.conbuildmat.2022.127775

23. Nunes GM, Anjos MAS, Lins ABS, Negreiros AMS, Pessoa L. 2023. Evaluation of the mechanical behaviour of representative volumetric elements of 3DCP masonry mixtures with partial replacement of cement by limestone filler and metakaolin. J. Build. Eng. 78:107650. https://doi.org/10.1016/j.jobe.2023.107650

24. ASTM/ISO 52939. 2023. Additive manufacturing for construction — Qualification principles — Structural and infrastructure elements. International Standard, Dec. 2023.

25. Han XY, Yan JC, Liu MJ, Huo L, Li JL. 2022. Experimental study on large scale 3D printed concrete walls under axial compression. Autom. Constr. 133:103993. https://doi.org/10.1016/j.autcon.2021.103993

26. Daungwilailuk T, Pheinsusom P, Pansuk W. 2021. Uniaxial load testing of large scale 3D printed concrete wall and finite element model analysis. Constr. Build. Mater. 275:122039. https://doi.org/10.1016/j.conbuildmat.2020.122039

27. Anjos MAS, Nunes GM, Lins ABS, Negreiros AMS, Pessoa L. 2024. Effect of the geometry of representative volumetric masonry elements: experimental and numerical analysis. Digital Concrete 2024 - Supplementary Proceedings, 2024.

28. Dias LS, Anjos MAS, Barbosa MS, Bezerra UT. 2024. Evaluation of mix design parameters based on basic constitutive relationships for 3DCP printing. Cerâmica 70:eZXBR6170. https://doi.org/10.1590/ZXBR6170

29. ABNT. 2016. NBR 13276: Argamassa para assentamento e revestimento de paredes e tetos – Preparo da mistura e determinação do índice de consistência. Rio de Janeiro.

30. ABNT. 2005. NBR 13278: Argamassa para assentamento de paredes e revestimento de paredes e tetos – Determinação da densidade de massa e do teor de ar incorporado. Rio de Janeiro.

31. ABNT. 2014. NBR 12118: Blocos vazados de concreto simples para alvenaria – Métodos de ensaio. Rio de Janeiro: 16.

32. ABNT. 2005. NBR 13279: Argamassa para assentamento e revestimento de paredes e tetos – Determinação da resistência à tração na flexão e à compressão. Rio de Janeiro.

33. ABNT. 2011. NBR 7222: Concreto e argamassa – Determinação da resistência à tração por compressão diametral de corpos de prova cilíndricos. Rio de Janeiro.

34. Wolfs RJM, Bos FP, Salet TAM. 2019. Hardened properties of 3D printed concrete: the influence of process parameters on interlayer adhesion. Cem. Concr. Res. 119:132-140. https://doi.org/10.1016/j.cemconres.2019.02.017

35. Ting GHA, Tay YWD, Qian Y, Tan MJ. 2019. Utilization of recycled glass for 3D concrete printing: rheological and mechanical properties. J. Mater. Cycles Waste: 21:994–1003. https://doi.org/10.1007/s10163-019-00857-x

36. ABNT. 2009. NBR 9778: Argamassa e concreto endurecidos – Determinação da absorção de água, índice de vazios e massa específica. Rio de Janeiro.

37. ABNT. 2005. NBR 15259: Argamassa para assentamento e revestimento de paredes e tetos – Determinação da absorção de água por capilaridade e do coeficiente de capilaridade. Rio de Janeiro.

38. Wolfs RJM, Bos FP, Salet TAM. 2018. Correlation between destructive compression tests and non destructive ultrasonic measurements on early age 3D printed concrete. Constr. Build. Mater. 181:447-454. https://doi.org/10.1016/j.conbuildmat.2018.06.060

39. Panda B, Lim JH, Tan MJ. 2019. Mechanical properties and deformation behaviour of early age concrete in the context of digital construction. Compos. Part B Eng. 165:563-571. https://doi.org/10.1016/j.

compositesb.2019.02.040

40. Roussel N, Buswell R, Ducoulombier N, Ivanova I, Kolawole JT, Lowke D, Mechtcherine V, Mesnil R, Perrot A, Pott U, Reiter L, Stephan D, Wangler T, Wolfs R, Zuo W. 2022. Assessing the fresh properties of printable cement based materials: high potential tests for quality control. Cem. Concr. Res. 158:106836. https://doi.org/10.1016/j.cemconres.2022.106836

41. Ollivier J P, Torrenti J M. 2014. A estrutura porosa dos concretos e as propriedades de transporte. In: Ollivier J P, Vichot A (Eds.). Durabilidade do concreto: bases científicas para a formulação de concretos duráveis de acordo com o ambiente. Cascudo O, Carasek H (Ed. trad.). 1. ed. São Paulo: IBRACON: 41–112.

42. Jaji MB, Zijl G, Babafemi AJ. 2024. Durability and pore structure of metakaolin based 3D printed geopolymer concrete. Constr. Build. Mater. 422:135847. https://doi.org/10.1016/j.conbuildmat.2024.135847

43. Li C. 2022. Relationship between water absorption and porosity in concrete with limestone powder addition. Struct. Concr. 23(5):3284-3293. https://doi.org/10.1002/suco.202100546

44. Chen Y, He S, Zhang Y, Wan Z, Çopuroğlu O, Schlangen E. 2021. 3D printing of calcined clay limestone based cementitious materials. Cem. Concr. Res. 149:106553. https://doi.org/10.1016/j.cemconres.2021.106553

45. Du J, Meng W, Khayat KH, Bao Y, Guo P, Lyu Z, Abu Obeidah A, Nassif H, Wang H. 2021. New development of ultra high performance concrete (UHPC). Compos. Part B Eng. 224:109220. https://doi.org/10.1016/j.compositesb.2021.109220

46. ABNT. 2016. NBR 6136: Bloco vazado de concreto simples para alvenaria estrutural – Requisitos. Rio de Janeiro.

47. Lim S, Buswell RA, Le TT, Austin SA, Gibb AGF, Thorpe T. 2012. Developments in construction scale additive manufacturing processes. Autom. Constr. 21:262-268. https://doi.org/10.1016/j.autcon.2011.06.010

48. Le TT, Austin SA, Lim S, Buswell RA, Law R, Gibb AGF, Thorpe T. 2012. Hardened properties of high performance printing concrete. Cem. Concr. Res. 42(3):558-566. https://doi.org/10.1016/j.cemconres.2011.12.003

49. Zhang Y, Zhang YS, She W, Yang L, Liu G, Yang Y. 2019. Rheological and harden properties of the high thixotropy 3D printing concrete. Constr. Build. Mater. 201:278-285. https://doi.org/10.1016/j.conbuildmat.2018.12.061

50. Duan Z, Li L, Yao Q, Zou S, Singh A, Yang H. 2022. Effect of metakaolin on the fresh and hardened properties of 3D printed cementitious composite. Constr. Build. Mater. 350:128808. https://doi.org/10.1016/j.conbuildmat.2022.128808

51. Wang Y, Chen M, Zhang T, Zhang M. 2024. Hardening properties and microstructure of 3D printed engineered cementitious composites based on limestone calcined clay cement. Cem. Concr. Compos. 152:105641. https://doi.org/10.1016/j.cemconcomp.2024.105641

52. Zareiyan B, Khoshnevis B. 2017. Effects of interlocking on interlayer adhesion and strength of structures in 3D printing of concrete. Autom. Constr. 83:212-221. https://doi.org/10.1016/j.autcon.2017.08.01